Electronic Supplementary Information for

Universal solid-state oxygen redox in antifluorite lithium oxides via transition metal doping

Hiroaki Kobayashi,*[a] Tetsuya Makimoto,[b] Yoshiyuki Ogasawara,[b] Kosuke Harada,[b] Masanobu Nakayama,[c] Mitsuhiro Hibino,[b] Tetsuichi Kudo,[b] Noritaka Mizuno[b] and Kazuya Yamaguchi[b]

a. Institute of Multidisciplinary Research for Advanced Materials, Tohoku University, 2-1-1 Katahira, Aoba-ku, Sendai, Miyagi 980-8577, Japan.
E-mail: h.kobayashi@tohoku.ac.jp

b. Department of Applied Chemistry, School of Engineering, The University of Tokyo, 7-3- 1 Hongo, Bunkyo-ku, Tokyo, 113-8656, Japan.

c. Department of Advanced Ceramics, Nagoya Institute of Technology, Gokiso, Showa, Nagoya, Aichi, 466-8555, Japan.

Section S1. Optimization of Ni-dopant sources and atomic ratio of Ni/(Li+Ni).

Fig. S1 shows voltage curves of NiDL cathodes prepared using NiO and $LiNiO_2$ as a Ni-dopant source with Ni/(Li+Ni) = 8%. The cathode synthesized from Li_2O and NiO exhibited larger overvoltage in charge and lower discharge capacity compared with the cathode synthesized from Li_2O and $LiNiO_2$.

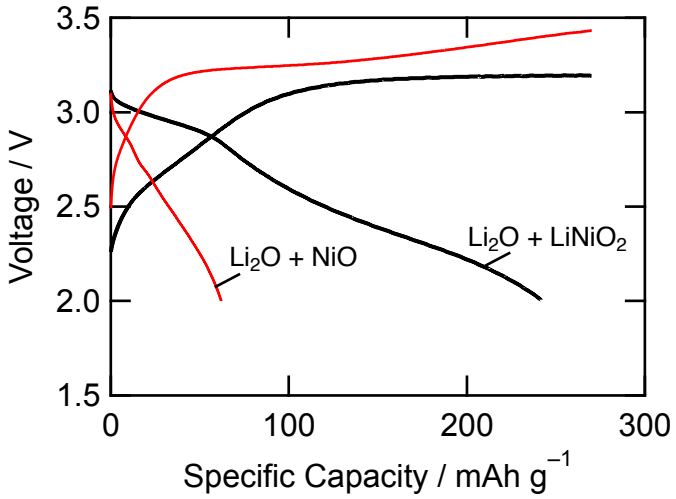

Fig. S1 Voltage curves of NiDL cathodes prepared using NiO or $LiNiO_2$ as a Ni-dopant source.

Fig. S2a shows XRD patterns of NiDL cathodes prepared from Li_2O and $LiNiO_2$ with various Ni contents. Peak intensity of the $LiNiO_2$-based phase gradually increases with increase in the Ni-content. Fig. S2b shows voltage curves. The cathode with Ni/(Li+Ni) = 8% exhibited the highest discharge capacity.

(a) (b)

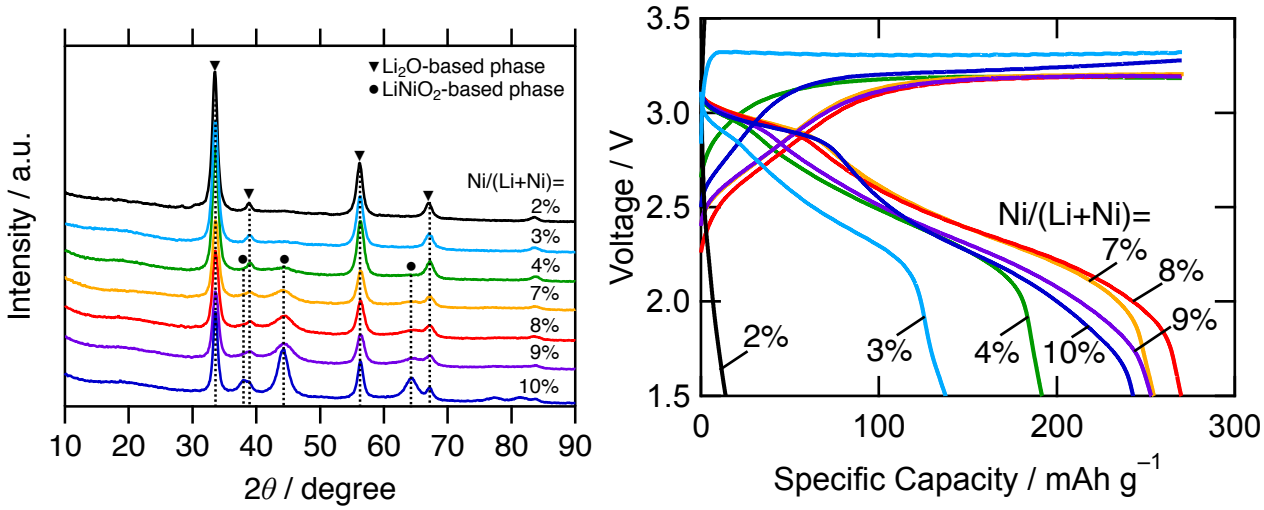

Fig. S2 (a) XRD patterns and (b) voltage curves of NiDL prepared from Li_2O and $LiNiO_2$ with Ni/(Li+Ni) = 2–10%.

Section S2. Particle size and surface morphology of NiDL particles.

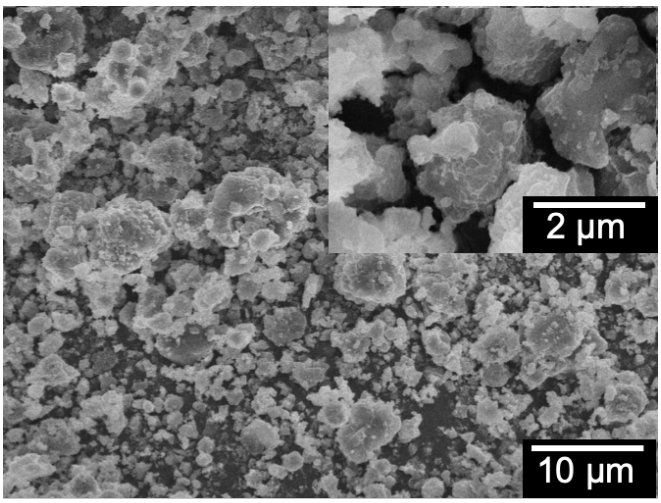

Fig. S3 SEM images of NiDL particles.

Section S3. Confirmation of Ni-doping to the cation site in the Li_2O structure.

To clearly understand the Li_2O-based phase, the sample with less amount of the $LiNiO_2$-based phase was investigated. We revealed that the sample with Ni/(Li+Ni) = 3% is suitable since its crystalline phase is almost the Li_2O-based phase, according to XRD patterns with the Rietveld refinement as shown in Table S1 and Fig. S4.

Table S1 Results of Rietveld refinement of NiDL with Ni/(Li+Ni) = 3%.[a]

Phase	Space group	Lattice parameters (Å)	Atom	Site	Occupancy (g)	Fraction (mol%)
NiDL	$Fm\bar{3}m$	a = 4.622(2)	Li	8c	g = 0.942(4)	97(1)
			Ni	8c	g = 0.0192(12)	
			O	4a		
$Li_xNi_{1-x}O$	$Fm\bar{3}m$	a = 4.106(9)	Li	4a	g = 0.49(9)	3(1)
			Ni	4a	g = 0.51(9)	
			O	4b		

[a] R_{wp} = 3.36%, R_p = 2.64%, R_e = 2.34%, S = 1.43.

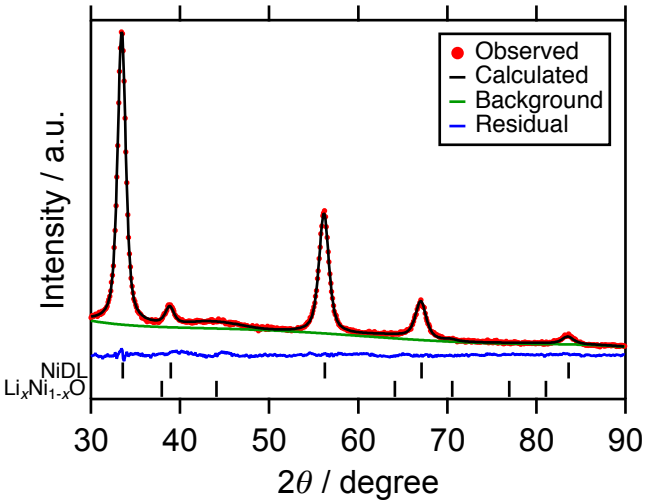

Fig. S4 XRD patterns of NiDL with Ni/(Li+Ni) = 3% and the fitting curve.

Fig. S5 shows pre-edge region in Ni *K*-edge XANES. In the region, Ni in the tetrahedral coordination, *e.g.*, $NiCr_2O_4$, exhibited a large peak corresponding to the dipole transition, whereas Ni in the octahedral coordination, *e.g.*, $Li_{1-x}Ni_xO$, exhibited a weak peak corresponding to the quadrupole transition. NiDL with Ni/(Li+Ni) = 3% showed a relatively large peak compared with $Li_{1-x}Ni_xO$, indicating the Ni coordination transformed from octahedral to tetrahedral. Since cation site in Li_2O is tetrahedral, Ni-doping into the cation site of Li_2O probably occurs.

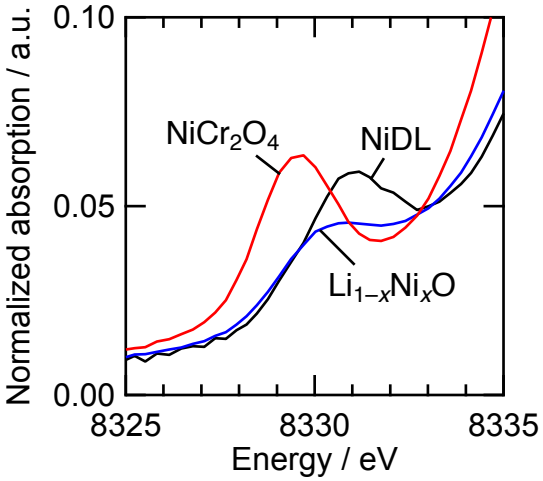

Fig. S5 Pre-edge region in Ni *K*-edge XANES.

Section S4. Transformation from hexagonal layered rocksalt $LiNiO_2$ to cubic cation-disordered rocksalt $Li_xNi_{1-x}O$ by the mechanochemical treatment.

Table S2 Results of Rietveld refinement of mechanochemically treated $LiNiO_2$.[a]

Phase	Space group	Lattice parameters (Å)	Atom	Site	Occupancy (g)
$Li_xNi_{1-x}O$	$Fm\bar{3}m$	a = 4.1142(8)	Li	4a	g = 0.445(6)
			Ni	4a	g = 0.555(6)
			O	4b	

[a] R_{wp} = 4.37%, R_p = 3.39%, R_e = 4.74%, S = 0.92.

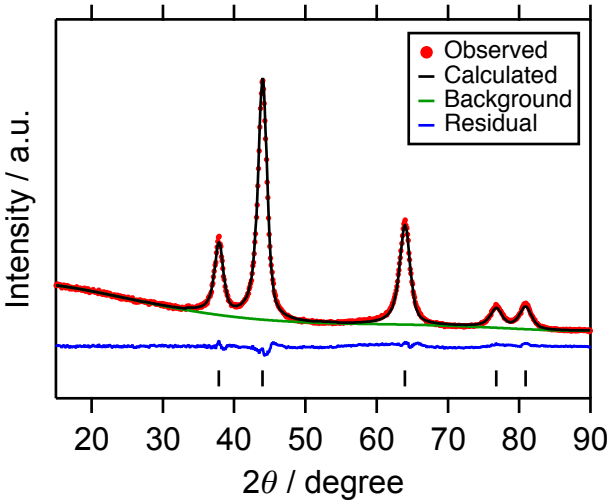

Fig. S6 XRD patterns of mechanochemically treated $LiNiO_2$ and the fitting curve.

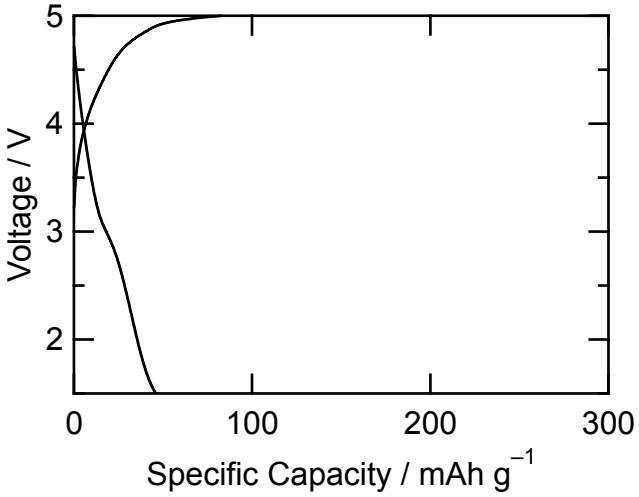

Fig. S7 Voltage curves of mechanochemically treated $LiNiO_2$.

Section S5. *In-situ* gas analysis with CoDL cathode during charge.

For the electrochemical cell, a two electrode beaker cell was used. CoDL cathode and Li foil anode were pressed on Al and Cu mesh current collectors, respectively. The electrodes were horizontally opposed with the glass fiber separator in between. The beaker cell, a circulation cylinder, and a 2-position 6-port valve with a sampling loop were assembled in an Ar-filled glove box. Then, the system was sealed, transferred outside, and connected to the gas flow system directly connected to a quadrupole mass spectrometer (OmniStar GSD301, Pfeiffer Vacuum). The gases in the cell were transferred to the sampling loop by using the circulation cylinder. For the analysis, the gases in the sampling loop were purged with a He carrier gas by switching the valve and transferred into the mass spectrometer. To remove a vapor of the electrolyte, the purged gases were passed through a cold trap (*ca.* –70 ºC). The amount of evolved O_2 (m/z = 32) and CO_2 (m/z = 44) were determined using the integrated peak areas of O_2 and CO_2 calibrated using that of Ar (m/z = 40), respectively.

(a)

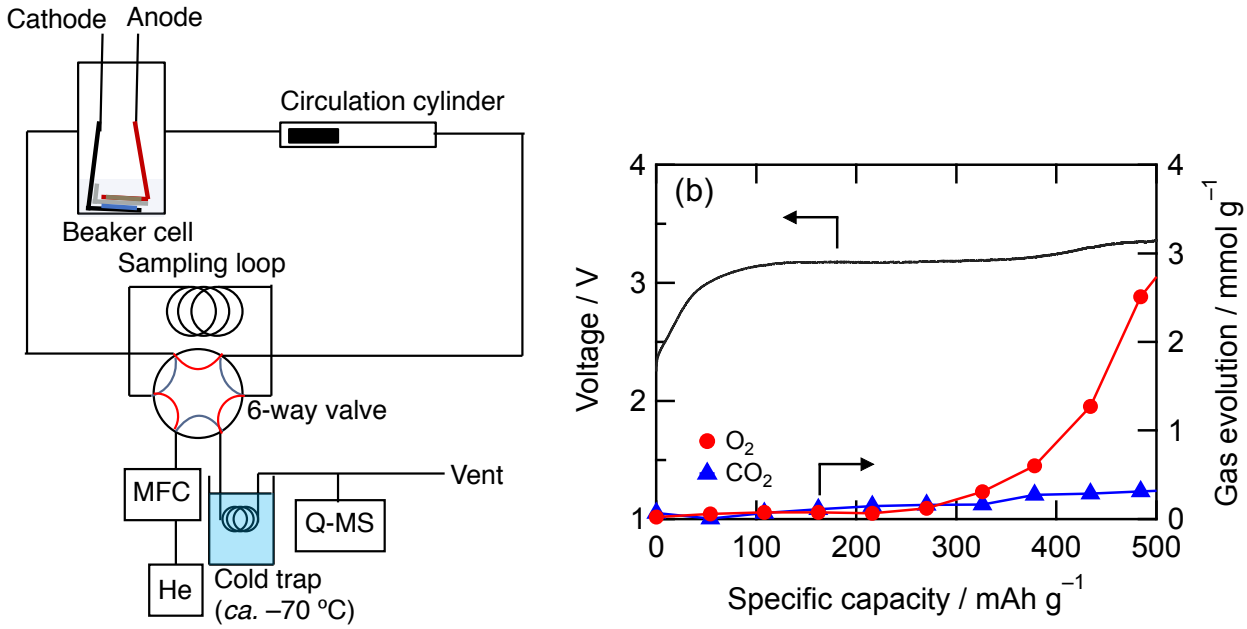

Fig. S8 (a) A schematic illustration of apparatus for the measurement of evolved gases. MFC: mass flow controller, Q-MS: quadrupole mass spectrometer. (b)Voltage curve of CoDL cathode and cumulative amounts of O_2 and CO_2 evolved in the charge process.

Section S6. First-principles band calculations of NiDL.

First-principles calculations based on the Heyd-Scuseria-Ernzerhof (HSEsol) hybrid functional[S1,S2] was performed to evaluate electronic structure of NiDL. We used Vienna ab-initio simulation package (VASP)[S3,S4] with modified Perdew-Burke-Ernzerhof generalized gradient approximation for solid (PBEsol-GGA)[S5,S6] and with the projector-augmented wave (PAW)[S7] method for density functional theory (DFT) part of hybrid functional. The composition and crystal structure were referred to the XRD-derived refined structure in this study, *i.e.* $Ni_1Li_{61}O_{32}$ in a simulation cell with 2 × 2 × 2 conventional cubic anti-fluorite unit cells. Total 5 structures with various Li/vacancy/Ni configurations in Li sites are generated in random manner and the lowest energy structure was chosen.

Fig. S9a and b presents projected density of states (PDOS) for the $NiLi_{61}O_{32}$ compounds. In Fig. S9b, oxygen PDOS corresponds to oxygen coordinated with Ni ions (4 ions). The valence bands ranging from –3 to 0 eV vs. Fermi level mainly consist of both localized O 2*p* orbital and hybridized orbital between Ni 3*d* and neighboring O 2*p*. Hole states arising from Ni 3*d* bands are clearly visible at ~2.5 eV vs. Fermi level with significant contribution of O 2*p* derived states in the PDOS diagram, indicating ligand hole formations. The calculated Bader charges[S8-S11] for Li, Ni, and O ions are listed in Table S3. The Bader charges of oxide ions bonded only with Li ions are almost –2, which corresponds to closed shell electron configuration. On the other hand, ligand hole formation is indicated from the Bader charges of oxide ions coordinated with Ni ions (–1.65). The valence bands and the hole states around Fermi level are visualized in Fig. S9c and d, respectively, where Ni-O hybridization is confirmed. Accordingly, the Ni-O bands play an important role for the redox reactions.

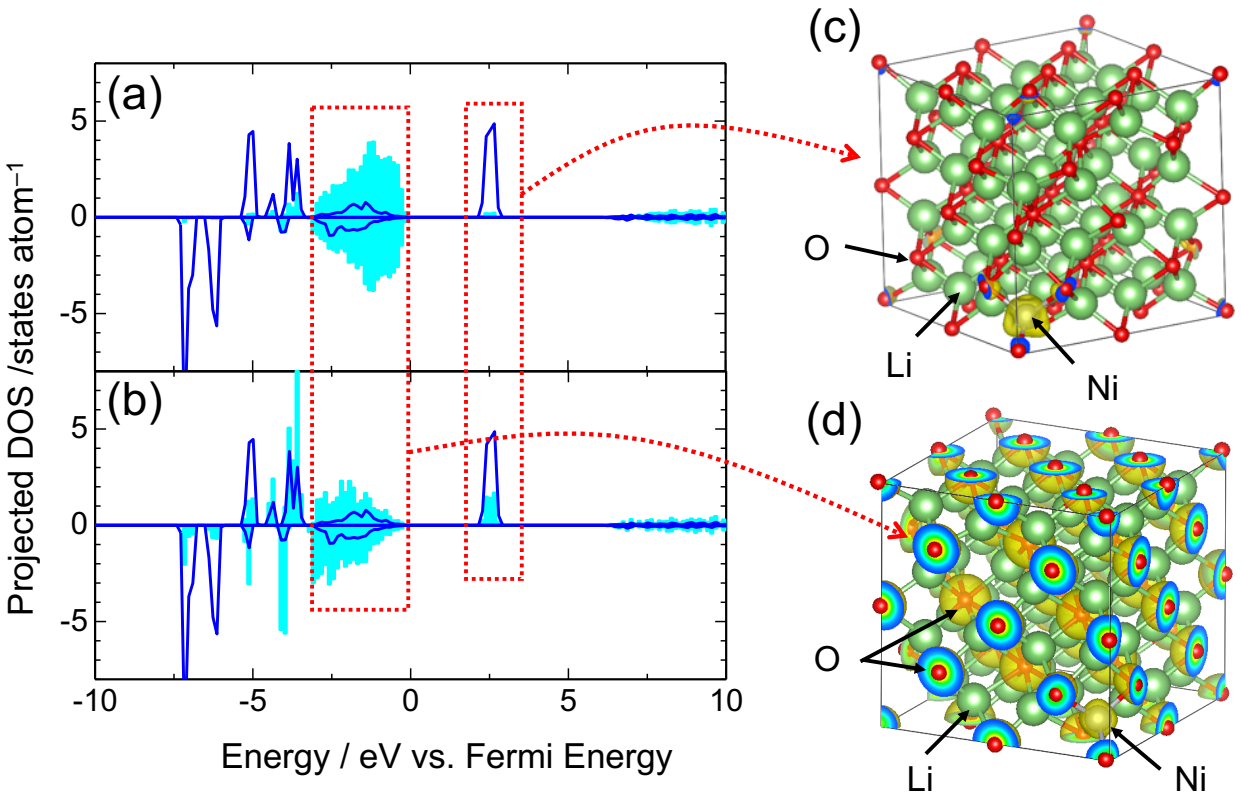

Fig. S9 (a), (b) Projected density of states (PDOS) for Ni (blue line) and O (light blue bar) ions in anti-fluorite type $NiLi_{61}O_{32}$ simulation cell. Oxygen PDOS in panel (b) corresponds to oxygen coordinated with Ni ions. (c), (d) Visualized electronic states for (c) hole states at ~ 2.5 eV and (d) valence band top at –3 to 0 eV vs. Fermi level by yellow-colored isosurfaces. Green-, gray-, and red-colored spheres correspond to Li, Ni and O ions, respectively.

Table S3 Averaged Bader charges for Li, Ni, and O ions. Label O1 and O2 represent the oxygen ions coordinated only with Li ions and with a Ni ion, respectively.

Ions (label)	Bader charge (averaged)
Li	1.00
Ni	1.52
O (O1)	–1.65
O (O2)	–2.00

Section S7. O *K*-edge XAS analysis of TMDL cathodes.

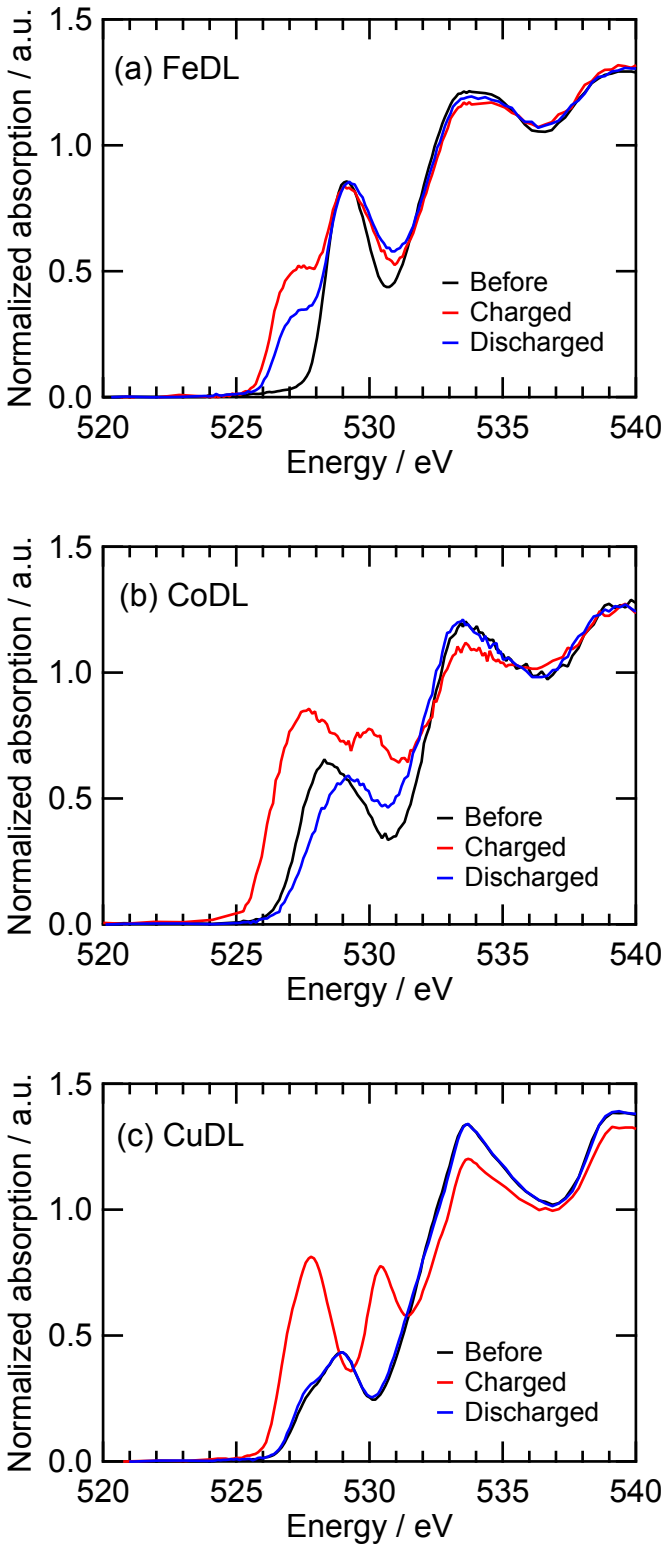

Fig. S10 O *K*-edge XANES spectra of TMDL cathodes during charge/discharge. The atomic ratio of TM/(Li+TM) was set to 10, 9, and 9% for FeDL, CoDL, and CuDL, respectively.

References

S1. J. Heyd, G. E. Scuseria and M. Ernzerhof, *J. Chem. Phys.,* 2003, **118**, 8207-8215.

S2. L. Schimka, J. Harl and G. Kresse, *J. Chem. Phys.,* 2011, **134**, 024116.

S3. G. Kresse and J. Furthmüller, *Phys. Rev. B,* 1996, **54**, 11169-11186.

S4. G. Kresse and J. Furthmüller, *Comp. Mater. Sci.,* 1996, **6**, 15-50.

S5. J. P. Perdew, K. Burke and M. Ernzerhof, *Phys. Rev. Lett.,* 1996, **77**, 3865-3868.

S6. J. P. Perdew, A. Ruzsinszky, G. I. Csonka, O. A. Vydrov, G. E. Scuseria, L. A. Constantin, X. Zhou and K. Burke, *Phys. Rev. Lett.,* 2008, **100**, 136406.

S7. P. E. Blöchl, *Phys. Rev. B,* 1994, **50**, 17953-17979.

S8. W. Tang, E. Sanville and G. Henkelman, *J. Phys.: Condens. Matter,* 2009, **21**, 084204.

S9. E. Sanville, S. D. Kenny, R. Smith and G. Henkelman, *J. Comp. Chem.,* 2007, **28**, 899-908.

S10. G. Henkelman, A. Arnaldsson and H. Jónsson, *Comp. Mater. Sci.,* 2006, **36**, 354-360.

S11. M. Yu and D. R. Trinkle, *J. Chem. Phys.,* 2011, **134**, 064111.